Internal stresses and voids in SiC particle reinforced aluminum composites for heat sink applications

M. Schöbel, W. Altendorfer, H.P. Degischer, S. Vaucher, T. Buslaps, M. Di Michiel, M. Hofmann

Internal stresses and voids in SiC particle reinforced aluminum composites for heat sink applications

M. Schöbel, W. Altendorfer, H.P. Degischer, S. Vaucher, T. Buslaps, M. Di Michiel, M. Hofmann

PII: S0266-3538(11)00048-0
DOI: 10.1016/j.compscitech.2011.01.020
Reference: CSTE 4915

To appear in: *Composites Science and Technology*

Received Date: 18 May 2010
Revised Date: 15 December 2010
Accepted Date: 23 January 2011

Please cite this article as: Schöbel, M., Altendorfer, W., Degischer, H.P., Vaucher, S., Buslaps, T., Di Michiel, M., Hofmann, M., Internal stresses and voids in SiC particle reinforced aluminum composites for heat sink applications, *Composites Science and Technology* (2011), doi: 10.1016/j.compscitech.2011.01.020

Internal stresses and voids in SiC particle reinforced aluminum composites for heat sink applications

M. Schöbel[1], W. Altendorfer[1], H.P. Degischer[1], S. Vaucher[2], T. Buslaps[3], M. Di Michiel[3], M. Hofmann[4]

[1]Institute of Materials Science and Technology, Vienna University of Technology, Karlsplatz 13, A-1040 Vienna, Austria

[2]Laboratory Materials Technology, EMPA, Feuerwerkstrasse 39, CH-3602 Thun, Switzerland

[3]European Synchrotron Radiation Facility, 6 Rue Jules Horowitz, F-38043 Grenoble, France

[4]Forschungsneutronenquelle Heinz Maier-Leibnitz, Lichtenbergstrasse 1, G-85747 Garching, Germany

Corresponding author: Michael Schöbel, Institute of Materials Science and Technology, Vienna University of Technology, Karlsplatz 13, E308, 1040 Vienna, Austria

Tel.: 004315880130836

Fax: 004315880130899

E-mail address: michaels@mail.tuwien.ac.at

Keywords: A. Metal-matrix composites; B. Thermal properties; B. Porosity/Voids; C. Residual stress; D. Non-destructive testing.

Abstract

Metal matrix composites (MMC) are being developed for power electronic IGBT modules, where the heat generated by the high power densities has to be dissipated from the chips into a heat sink. As a means of increasing long term stability a base plate material is needed with a good thermal conductivity (TC) combined with a low coefficient of thermal expansion (CTE) matching the ceramic insulator. SiC particle reinforced aluminum (AlSiC) offers the high TC of a metal with the low CTE of a ceramic. Internal stresses are generated at the matrix-particle interfaces due to the CTE mismatch between the constituents of the MMC during changing temperatures. Neutron and synchrotron diffraction was performed to evaluate the micro stresses during thermal cycling. The changes in void volume fraction, caused by plastic matrix deformation, are visualized by synchrotron tomography. The silicon content in the matrix connecting the particles to a network of hybrid reinforcement contributes essentially to the long term stability by an interpenetrating composite architecture.

1. Introduction

Power electronic devices such as IGBT (Insulated Gate Bipolar Transistor) modules are used as converters in hybrid vehicles or railway traction [1]. High power densities generate heat which has to be transported from the ceramic chips through the ceramic substrate, the solder and the base plate into a heat sink. Conventional base plate materials such as Cu or Al**,** with a high thermal conductivity (TC)**,** do not fulfill the requirements of a matching coefficient of thermal expansion (CTE) in order to avoid delamination of the solder during temperature changes. For this purpose metal matrix composites are being developed which combine the high TC of a metal with the low CTE of a ceramic. SiC particle reinforced aluminium (AlSiC) has recently been introduced as base plate material [2]. The long term stability under service conditions of such composites is important and has to be guaranteed. Dense particle packing of SiC particles in AlSiC cause significant micro stresses between the particles and the matrix

during temperature changes [3]. This is due to the CTE mismatch between the Al in the matrix (23 - 30 ppm/K) and SiC (6 ppm/K) which may cause delamination between the MMC constituents. However, voids are already present in gas pressure infiltrated AlSiC samples after processing. The anomalous CTE results [4] are compared with thermo-elastic calculations [5] for an AlSi7Mg/SiC/70p composite as illustrated by a simplified diagram in Fig. 1. The Turner model assumes an interconnected reinforcement that is provided by Si bridges between the particles [4]. The difference above 200 °C was explained by stress induced void closure during heating and reopening after cooling [6]. The CTE(T) curve of the composite was simulated using a 2D elasto-plastic FE model allowing a stress induced reduction of the void volume fraction in an AlSi7Mg/SiC/70p composite [7]. The aim of this work was to determine the internal stresses in AlSiC and to correlate them with the void kinetics and the resulting CTE behavior. Synchrotron and neutron diffraction was performed to determine the in-situ micro stresses occurring during thermal cycling. High resolution in-situ synchrotron tomography is used to investigate delamination and void kinetics producing thermal fatigue damage. Pure Al as well as AlSi7 matrix composites with different particle size distributions were tested and the effects on reinforcement architectures described in [8] could be revealed.

2. Experimental methods

2.1. Materials description

The same composite was used for dilatometer tests in previous work [4] showing the mentioned anomalous CTE behavior above 200 °C. In order to avoid mechanical finishing after infiltration the Al/SiC/60-70p and AlSi7/SiC/60-70p composites with monomodal (Ø ~ 50µm) or bimodal (Ø ~ 5 + 50 µm) SiC particles were squeeze cast by EMPA [9] in defined dimensions for the neutron and synchrotron experiments. Fig. 2 shows the SiC particles and the AlSi12 eutectic between the α-Al dendrites. The matrix of Al/SiC/60p consists of Al

grains only, which did not react with SiC owing to the fast infiltration process. The composite without Si in the matrix disintegrates by deep etching and the SiC particles fall apart, but with 7 % Si content an interconnected reinforcement network (Si-SiC) remains in shape after removal of the α-Al (Fig. 3). Si bridges connecting the reinforcements to a network were identified similar to those of the AlSi7Mg/SiC/70p composite [4, 6] produced by gas pressure infiltration of a trimodal size distribution Ø ~ 3 – 80 µm of SiC particles [10] by ELECTROVAC/Austria. Mg has been added to provide some precipitation hardening of the matrix, which does not influence the reinforcement structure.

2.2. In-situ diffraction experiments

Strain measurements were made using synchrotron radiation travelling through the composite samples during thermal cycling [11, 12]. The measurements on AlSi7Mg/SiC/70p were performed on ID15A, ESRF, Grenoble [http://www.esrf.fr] using the white beam diffraction setup and two energy dispersive (EDS) Ge-detectors for the two orthogonal reflecting lattice directions relative to the sample [6]. Complete diffraction patterns were acquired within ~ 2 min simultaneously to micro tomography. The gauge volume ~ 1 mm³ covered the sample diameter (10 x 1.5 x 1.5 mm³) completely by rotating the sample in the beam to increase grain statistics. Diffraction on reference samples of the constituents during thermal cycling provided the $d_0(T)$ necessary for strain calculations. Fig. 4 shows the diffraction pattern of the composite with the corresponding reference scans at RT. The α-Al and Si in the matrix and the SiC particles were identified by their typical lines. Hexagonal contributions (SiC_h) could be identified in the SiC as well but were not taken into account for strain calculation. Some Al lines appear in the SiC particle reference as well due to the powder container made of Al used for diffraction. The marked region of interest (ROI) represents the range in d-space of the compared neutron measurement described in the following.

Strain measurements with an energy dispersive synchrotron setup are more difficult due to the small gauge volume enclosing only a few grains. Therefore neutron diffraction was used for measurements on the coarse grained matrix of Al/SiC/60p and AlSi7/SiC/60p. Samples were produced for neutron diffraction in cylindrical shape (d ~ 6mm, h ~ 10mm). Neutron experiments were carried out on the Stress Spec instrument at FRM2 Garching [http://www.frm2.tum.de, 13]. A monochromatic neutron beam (λ = 1.67 Å) travelling through the sample generates the {h k l} specific diffraction cones acquired by a 2D ^{3}He position sensitive detector (PSD) system. Acquisition times ~ 3 min were sufficient due to the large gauge volume of 5 x 5 x 5 mm³ and high monochromatic neutron flux of ~ 2 x 10^7 n cm^{-2} s^{-1} on the sample. Fig. 5 shows the Debye Scherrer cones of the observed {h k l} reflections of Al {3 1 1} and of SiC_c {3 1 1} from the polycrystalline sample. A segment of the diffracted cones is projected on the 2D PSD plate. The dominating crystal orientation in the coarse grained matrix produces vertical intensity fluctuations in the Al {3 1 1} diffraction cone. Diffraction patterns of selected peaks of the components were acquired during thermal cycling of the composites. The example of the summed intensities along the Debye Scherrer cones recorded at RT is presented in Fig. 6.

The strains were determined by in-situ neutron diffraction of the composite and its constituents [6] comparable to the synchrotron diffraction but in a smaller d-space range (ROI shown in Fig. 4). Exactly the same setup and sample dimensions were taken for the MMC, the matrix reference and the particle powder container. The samples' diameters were flooded completely by the incoming beam of the synchrotron and also by the neutrons in order to average out macro strains in the samples during thermal cycling and size effects on peak shape. The temperature gradients of the furnace setup for composite as well as for reference samples were neglected.

Strain calculation was made from synchrotron and neutron diffraction data in the same way. Fig. 7 shows temperature dependence of d-spacing of two dominant matrix peaks Al {2 0 0} and Al {3 1 1} in the composite and the AlSi7Mg reference which were taken from the synchrotron data. The slightly larger d-value in the composite's matrix is reduced during heating ending up smaller than in the matrix reference above 200 °C. The Al {3 1 1} reflection shows a strain hysteresis in the composite due to contributions of plastically deformed matrix material. The hysteresis of the reference in Al {3 1 1} due to interfacial strains between the α-Al and Si in the matrix are included in the reference as well and therefore not taken into account for the results of the composite's stresses. The AlSi7 matrix was chosen to eliminate these stresses and the d-space variations owing to increasing solubility of Si during heating. The resulting strain values represent the stresses in the phases of AlSi7 matrix produced by the Si-SiC reinforcement architecture only. Strain calculation in the composites was made relative to reference measurements. The strains were calculated from the synchrotron measurement using equ. (1a) with the composite's peak energies e(T) in the EDS-spectra relative to the reference $e_0(T)$. Equ. (1b) delivered the strains from neutron diffraction with composite's peak angles θ(T) in the PSD-spectra relative to the reference $\theta_0(T)$.

$$\varepsilon(T) = \frac{e_0(T) - e(T)}{e(T)} \tag{1a}$$

$$\varepsilon(T) = \frac{\sin\theta_0(T) - \sin\theta(T)}{\sin\theta(T)} \tag{1b}$$

EDS peak's energy e(T); PSD peak's angle θ(T); Strain ε(T); Temperature T

The spherical symmetry of averaged micro strains (gauge volume >> particles size) in and around the particles simplifies the orthogonal stresses from equ. (2a) to isotropic ones according to equ. (2b).

$$\sigma_i = \frac{E(T)\cdot\varepsilon_i(T)}{(1+\upsilon)} + \frac{E(T)\cdot\upsilon\cdot\left(\varepsilon_1(T)+\varepsilon_2(T)+\varepsilon_3(T)\right)}{(1+\upsilon)\cdot(1-2\upsilon)} \quad (2a)$$

$$\sigma = \frac{E(T)\cdot\varepsilon(T)}{(1-2\upsilon)} \quad (2b)$$

Young's modulus E; Poisson's ratio υ; Strain ε; Stress σ; Temperature T

An isotropic assumption is supposed by the result of synchrotron diffraction in two principal stress directions as shown in Fig. 8, which will be discussed later. Neutron diffraction geometry using unidirectional scans was decided to be sufficient for micro strain determination.

2.3. Fast synchrotron tomography

Synchrotron tomography offers the possibility to investigate thermal fatigue damage in metal matrix composites [14]. High resolution as well as a short acquisition time on ID15A at ESRF Grenoble enabled in-situ scans during thermal cycling simultaneously to the diffraction analysis. A white beam was used producing absorption contrast images of the sample acquired by a high resolution CCD camera behind the sample. The ~ 1000 projections of the sample during rotation (180 °) were reconstructed to a 3D volume with a voxel size of ~ (1.4 µm)³. The acquisition time for one complete tomography scan using the white beam was ~ 10 min.

Tomography on ID19 at ESRF Grenoble delivered a more accurate absolute value of void volume fractions due to higher resolution. Scans comparable to neutron diffraction on Stress Spec at FRM2 Garching were made with the same composites and conditions, but different samples' shapes. AlSiC has been infiltrated in 10 x 0.8 x 0.8 mm for tomography to achieve a voxel size of (0.6 µm)³ in a region of interest scan of a 0.6 x 0.6 x 0.3 mm³ volume. A parallel monochromatic beam setup with low energies (~ 15 keV) was used for good absorption contrast of matrix, particles and voids. The samples were rotated 180 ° in the beam and the projections were reconstructed to a 3D image similar to the experiments on ID15A. The detector set at high resolution was operated in binning mode to reduce the acquisition time of one scan down to 3 min, which is the same as for neutron diffraction.

The contrasts of the voids and cracks in the matrix were quantified by a feasible threshold value for segmentation in the RT tomogram. The same threshold value was delivered by the 'getAutoThreshold' function of the ImageJ software tool [http://rsbweb.nih.gov/ij]. The same histogram threshold was used for segmentation of voids in all images to investigate relative changes in void volume fractions. It is assumed that the relative changes are not affected by image resolution or by reconstruction artefacts. The absolute values determined are to be considered with respect to the same visibility criterion. The detectability of voids is limited to Ø > 3 voxel, i.e. 4 µm and 2 µm for ID15A and ID19 tomograms, respectively. The samples' drift between scans due to thermal expansion of the furnace setup was corrected by 3D image registration [15] to investigate regions of interests in the micro tomography scans.
Visualization of changes in volume and shape of single voids during thermal cycling can be visualized by voxel to voxel correlation in the different scans after 3D translation and rotation correction of the images.

3. Results

Energy dispersive synchrotron X-ray diffraction delivered diffraction patterns including several {h k l} planes simultaneously (Fig. 4). The strain values were determined relative to reference measurements on matrix samples (Fig. 7). The {h k l} specific strains in the matrix (α-Al, Si) and in the SiC particles are shown in Fig. 8. The orientation independent strains prove the assumption of strain isotropy in the gauge volume (0.3 x 0.3 x 1.5 mm³) in directions 0 ° and 90 ° relative to the sample. The elastic strain amplitude of Si is bigger than that of the surrounding Al of low yield strength. The strains in both phases remain more less the same above 300 °C. The SiC particles do not show a significant thermal strain evolution due to their high elastic modulus and high volume fraction of 60 to 70 vol.%. A more accurate calculation of error (compared to previous results [6]) was achieved by implementation of several peaks and orientations. Matrix micro stresses during thermal cycling are presented in Fig. 9. High hydrostatic compression during heating and tension builds up during cooling within the matrix. The eutectic Si has similar stress behavior as α-Al influenced by the Si-SiC reinforcement. Decreasing stresses can be observed in the Si as soon as 400 °C is surpassed (A), while the stress amplitude in the α-Al remains almost constant > 300 °C. The matrix micro stresses appear slightly lower in amplitude after 5 thermal cycles compared to the first cycle. The same micro stress decrease (A) in the Si can be observed when passing 400 °C after 5 cycles. The compressive stress in the Al matrix vanishes during cooling (B) inverting into tension at RT, whereas the transition from compression to tension of Si occurs continuously above RT.

Neutron diffraction was made on four composite types with two different matrices and two particle size distributions. Large gauge volumes were necessary for the coarse grained structure of the squeeze cast Al/SiC and AlSi7/SiC with volume fractions of 60 vol.% monomodal and 70 vol.% bimodal SiC particles (Fig. 2). The effect of coarse grained matrix is shown in Fig. 5 by the variations in intensities taken from a cubic volume of 5 x 5 x 5 mm³.

The Al {3 1 1} and SiC_c {3 1 1} peak intensities were summed along the recorded sections of the Debye Scherrer rings. The resulting peak positions were determined at several temperatures, from which the strains were calculated relative to stress free reference measurements. Peak offsets were eliminated by $\Sigma\sigma_i(T) = 0$ over both thermal cycles. Surface effected peak shifts of the small samples (< gauge volume) could be neglected. The stress calculation was made using equation (2b) assuming an isotropic strain state as shown in the synchrotron experiments on AlSi7Mg/SiC/70p (Fig. 8). The micro stresses in the Al-matrix and in SiC were calculated for monomodal and bimodal particle systems (Fig. 10). The error is represented by the peaks' standard deviation [11, 12]. Matrix stresses of the Al in AlSi7 are similar to those in Al of the AlSi7Mg matrix from the synchrotron results (Fig. 10c, 10d vs. 9) with a step of zero stress during cooling (B). The stress evolution in pure Al matrix during thermal cycling (Fig. 10b) can be interpreted only by a similar tendency as of the AlSi7 matrix (Fig. 10c), but with small compression during heating and little tension during cooling. There is no difference in the stress evolution in Al between monomodal and bimodal particle distributions (Fig. 10c, 10d). The temperature dependence of the neutron diffraction results for AlSi7 with bimodal SiC particle distribution is similar to the synchrotron measurements of the trimodal SiC distribution. A low stress amplitude**,** independent from the particle distribution, is confirmed for SiC by neutron diffraction.

In-situ synchrotron tomography was performed on ID15A simultaneously to synchrotron diffraction [6] and on ID19 complementary to neutron diffraction (FRM2) [16]. Voids mainly at the interfaces between SiC particles and Al matrix could be visualized by both beam conditions. A change of their volume fraction by stress induced visco-plastic matrix deformation was observed. Individual voids were visualized during thermal cycling after image registration [15] of the high resolution synchrotron tomography scans. A single void between large SiC particles is shown in Fig. 11 during heating and cooling. The volume of a

single void cluster (Ø ~ 30 µm) changes comparably to the results taken from a void segmented from an ID15A tomogram shown in Fig. 12c by about a factor of 5. The void volume fraction of a more representative sample region of ~ 0.3 mm³ decreases by ~ 75 % from room temperature to 400 °C as shown in Fig. 12b taking into account only voids bigger than 4 µm in diameter due to a voxel size of (1.4 µm)³. Fig. 13 shows a group of voids, which increase 10 times in volume after 25 cycles forming connected voids in between SiC particles. This represents severe thermal fatigue damage at the interfaces.

Synchrotron tomography on ID19 with a parallel monochromatic beam setup and (0.6 µm)³/voxel was made on Al/SiC/60p and AlSi7/SiC/60p (both with monomodal SiC) complementary to neutron diffraction. The volume fraction of voids > 1 µm were segmented by in-situ tomographies during the first cycle RT – 350 °C – RT from a representative sample region of (0.3 mm)³. In the AlSi7 matrix the identified void volume fraction decreases from 1.7 vol.% to 0.8 vol.% during heating and increases to 1.3 vol.% after cooling again as shown in Fig. 14. In pure Al matrix, voids decrease from 1.8 vol.% to 1.1 vol.% during heating but do not reopen completely after cooling. The corresponding 3D image views of an Al/SiC/60p cube with the same voids segmented at RT and at 350 °C are shown in Fig. 15. The voids are mainly arranged at the interfaces and shrink as shown in Fig. 14 during heating in the pure Al matrix composite due to the big CTE mismatch at the interfaces.

4. Discussion

The big CTE mismatch (ΔCTE) between Al, Si and the reinforcement produces internal stresses in SiC particle reinforced aluminium composites during changing temperatures. The investigated AlSiC samples are produced by infiltration of densely packed particle preforms, which are compressed further by the non-wetting Al melt [10]. Assuming a stress free state at the solidification temperature (neglecting the liquid-solid shrinkage), the matrix in between

the rigid SiC particle preform needs to shrink according to the volume difference equ. (3). (3a) refers to particles embedded in the matrix, whereas (3b) refers to a 3D rigid reinforcement structure as present in AlSi7 matrices where Si forms bridges between densely packed SiC particles. The solidus temperature for AlSi7Mg is 575 °C. The average ΔCTE between Al and SiC amounts to 20 ppm/K, yielding a volume mismatch in Al/SiC/60p according equ. (3a) of ~ 2 vol.% when cooled from solidification to room temperature. Applying equ. (3b) to AlSi7/SiC/60p yields a volume misfit of ~ 1.3 vol.% during cooling from 575 °C.

$$\Delta V(\Delta T) = 3v_r \cdot \left|CTE_m - CTE_r\right| \cdot \Delta T \quad \text{(3a)}$$

$$\Delta V(\Delta T) = 3v_m \cdot \left|CTE_m - CTE_r\right| \cdot \Delta T \quad \text{(3b)}$$

Volume change ΔV, Temperature change ΔT, Volume fraction ν

Suffix: Matrix m, Reinforcement r

Such shrinkage effects cannot be accommodated completely by elastic straining. Therefor 1 – 2 vol.% voids will be formed by hydrostatic tension in the matrix between the particles, even if infiltration had been perfect. Those voids change their volume during thermal cycling. Visco-plastic matrix deformation results from internal micro stresses close to the matrix yield strength decreasing with increasing temperature. The expanding matrix moves into the voids almost closing them during heating when the particles cannot move and reopens them by tension during cooling again. An initial void volume fraction of > 1 vol.% at room temperature in the AlSi7Mg matrix is reduced by 80 % at 400 °C by high hydrostatic compression up to ~ 200 MPa in Al (Fig. 9, 12). The high hydrostatic micro stresses in Al are explained by the presence of a connected network of Si bridges between the SiC particles [6]. An interpenetrating composite is formed during eutectic solidification of the matrix between

the densely packed particles. The Si-SiC network shrinks by 1.5 vol.% less than the Al-matrix in between during cooling and expands by the same amount less during heating. Assuming bonding of the Al, then elastic strains will reduce the volume mismatch. The maximum elastic strains in Al at room temperature were measured to be around 0.1 % for an yield strength of ~ 70 MPa. Since there is no real hydrostatic tension condition in the Al matrix owing to the irregular shape of the reinforcement, at least 1 vol.% of voids can be expected in even perfectly infiltrated AlSi7/SiC/>55p [3] composites at RT. The void volume fraction measured at RT by high resolution synchrotron tomography amounts to > 1.2 vol.% of voids > 1 µm in diameter (Fig. 14). Thus an almost perfect infiltration quality can be concluded. The lower volume of 0.15 vol.% measured at ID15A (Fig. 12) with $(1.4\ \mu m)^3$ voxel size refers only to voids > 4 µm in diameter. In both cases the void volume fraction is reduced during heating by the inversion of the tensile matrix stress at RT after cooling, to compression at around 200 °C. The ID15A tomograms reveal, that only 20 % of the voids > 4 µm remain at 400 °C compared to RT. The ID19 tomograms of AlSi7/SiC/60p indicate, that only < 50 % of the voids > 1 µm remain at 350 °C corresponding to a reduction of the void volume fraction from > 1.7 vol.% to < 0.8 vol.%. High resolution tomograms reveal that the voids close during heating due to visco-plastic matrix deformation by compressive stresses determined by diffraction. This reduction of the void volume fraction**,** by internal accommodation of the increasing matrix volume**,** explains the observed anomalous CTE(T) decrease above 200 °C (Fig. 1) [4] which could not be explained by the thermo elastic model [5]. The stress levels in Al and Si undergo a reproducible step in the reduction of compressive stresses > 200 °C (marked “A” in Fig. 9) during cooling. The Si bridges between the SiC particles suffer tension as soon as the Al expands in the Si-SiC network. The superposition of compression of Si particles embedded in the Al matrix with the longitudinal tension of the Si bridges between the SiC particles is assumed to be the reason for this step before the stress reduces during cooling. The zero stress level in Al, around 200 °C during cooling (“B” in Fig. 9, 10) is

associated with the reopening of the pores during shrinkage of the Al. Further cooling to RT produces matrix tension reopening the voids more by plastic straining. The 2D unit-cell-model [7] of 70 vol.% SiC connected by 1.6 vol.% Si filled with 28.4 vol.% Al, containing 0.25 vol.% voids at RT, considers only the deformation of the free surface of the Al-matrix along the void, but does not allow debonding from the SiC particle. The volume of a void in that MMC was calculated to increase by 50 % of its initial volume at 500 °C when cooled to RT. When comparing the thermal cycles of Al in the matrix, with and without Si, the internal stresses are much less in the pure Al matrix composite (Fig. 10). The tendency is the same, compression during heating, tension during cooling. The void volume fraction in Al/SiC/60p reduces by 30 % during heating. In the pure Al matrix a system of touching particles exists which cannot follow the shrinkage of the matrix. If the interface bonding is strong then movement of particles by the expanding metal matrix during heating is hindered by touching neighboring particles, even when they are not connected by Si bridges [16]. Therefor equ. (3a) does not represent the situation. The void volume fraction increases with the number of thermal cycles indicating that debonding advances by low cycle fatigue damage mechanisms. After 25 cycles strong thermal fatigue damage can be observed through an increase of the void volume fraction of up to 10 times of the initial value (Fig. 13). After 5 cycles the micro stress amplitude is reduced in AlSi7Mg/SiC/70p (Fig. 9). The increase in the void volume fraction occurs faster in the Si free Al matrix than in those with Si-SiC networks. Similar micro stresses were observed in AlSi7/SiC/60p with monomodal SiC as well as in AlSi7/SiC/70p with bimodal SiC particle distributions [17] by in-situ neutron diffraction (Fig. 10). The increase of the stress amplitude in Al with increasing SiC volume fraction is within the scatter range. The SiC particle stresses are not detected to compensate the matrix stresses inversely.

5. Conclusions

- Metal matrix composites with densely packed ceramic particles contain a certain volume fraction of voids after cooling from the processing temperature. This is due to the large CTE mismatch between the constituents resulting in the elasto-plastic and viscous deformation of the ductile matrix.
- Al matrices with Al-Si eutectic solidify after melt infiltration of the particle preform forming an interpenetrating composite consisting of a network of ceramic particles connected by rigid Si bridges.
- The Al matrix suffers hydrostatic tensile stresses after cooling from processing. During reheating the stress inverts into hydrostatic compression to significantly higher levels within Si-SiC networks than in pure AlSiC composites.
- During reheating the voids close partly by viscous flow of the matrix and reopen plasticly during further cooling, parallel to the micro stress oscillations.
- The void kinetics during thermal cycling reduces the CTE at elevated temperatures, where creep of the matrix becomes effective. Voids influence the macroscopic CTE behavior by allowing for plastic deformation of the softer phase.
- Thermal cycles exceeding 150 K imposed on AlSiC represent low cycle fatigue exposure on the Al matrix at the interfaces with the rigid reinforcement producing debonding, which increases with the number of cycles. The damage advances significantly faster in pure Al matrix than in composites with Al-Si eutectic.

Acknowledgements

The research was financed by the ExtreMat 6th framework EU project, and the authors would like to thank all the cooperating partners. Also thanks owing to Mr. A. Rhyswilliams for his language corrections during finalization of the work. Last but not least we would like to thank the helpful support from the staff of ESRF Grenoble France and FRM2 Garching Germany helping organizing and carrying out successful experiments on their sites.

References

[1] Zweben C, Metal-matrix composites for electronic packaging. J Metal 44: 15-23, 1992.

[2] Lefranc G, Degischer HP, Sommer HK, Mitic G, In: Massard T, editor. ICCM12 proceedings, Paris, electronic support; 1999.

[3] Elomari S, Boukhili R, San Marchi C, Mortensen A, Lloyd DJ. J. Mater. Sci. 32: 2131 – 2140, 1997.

[4] Huber T, Degischer HP, Lefranc G, Schmitt, Comp Sci Technol 66: 2206-17, 2006.

[5] Turner P, J Re. Nat. Bu. Stan. 36: 239-50, 1946.

[6] Schöbel M, Requena G, Kaminski H, Degischer HP, Mat. Sci. For. vol. 571-572, 413-418, 2008.

[7] Nam TH, Requena G, Degischer HP, Comp.: Part A 39: 856-865, 2008.

[8] Schöbel M, Fiedler G, Degischer HP, Altendorfer W, Vaucher S, Adv. Mater. Res. 59: 177-181, 2009.

[9] Beffort O, Long S, Cayron C, Kuebler J, Buffat PA, Comp. Sci. Tech. 67: 737-745, 2007.

[10] Michaud VJ, Suresh S, Mortensen A. Fundamentals of Metal Matrix composites. Butterworth-Heinemann, Boston, 1993.

[11] Fitzpatrick ME, Lodini A. Analysis of Residual Stress by Diffraction using Neutron and Synchrotron Radiation. Taylor & Francis, London, 2003.

[12] Hauk V. Structural and Residual Stress Analysis by Nondestructive Methods. Elsevier B.V. Amsterdam, NL, 1997.

[13] Hofmann M, Skirl S, Pompe W, Rödel J, Acta Mater. 47: No. 2, pp. 565-577, 1999.

[14] Terzi S, Salvo L, Suéry M, Limodin N, Adrien J, Maire E, Pannier Y, Bornert M, Bernard D, Felberbaum M, Rappaz M, Boller E, Scrip. Mat. 61: 449-452, 2009.

[15] Altendorfer W. Void tracking in SiC particle reinforced Al, Diploma Thesis, Institute for Computer Graphics and Algorithms, TU Vienna, Austria, 2008.

[16] Schöbel M, Degischer HP, Vaucher S, Hofmann M, Cloetens P, Acta Mat. 58: Iss. 19, 6421-6430, 2010.

[17] Molina JM, Narciso J, Weber L, Mortensen A, Louis E, Mater. Sci. and Eng. A: 480, 2008.

Figures

Fig. 1: CTE of AlSi7Mg/SiC/70p between 50 and 500 °C with an anomalous decrease above 200 °C [4] compared to the calculated value [5] for AlSi7 matrix with 70 vol.% SiC particles interconnected.

Fig. 2: LOM images of AlSi7/SiC/70p composite (a) monomodal (b) bimodal. Dark SiC particles are embedded in a bright AlSi7 matrix with Si in the interdendritic eutectic (grey).

Fig. 3: SEM images of deep etched AlSi7/SiC/60p (a) monomodal SiC (b) bimodal SiC composites as shown in Fig. 2. Si connects the particles to a network of reinforcements.

Fig. 4: EDS spectra of synchrotron diffraction at RT of the composite (a) compared with reference measurements of the matrix (b) and the reinforcement particles (c). The ROI represents the d-space range investigated by neutron diffraction in Fig. 6.

Fig. 5: The neutron diffraction geometry with Debye Scherrer cones behind the sample. The 2D ^{3}He PSD detector on Stress Spec, FRM2 shows segments of the projected cones.

Fig. 6: Vertical sum over the 2D detector image delivers selected {h k l} neutron reflections at a fixed 2θ window of the composite and a reference. The composite (a) compared to Al matrix (b) and SiC powder (c).

Fig. 7: Changes in matrix d-space during thermal cycling (RT – 400 °C) in the Al {2 0 0} and Al {3 1 1} lattices. The composite shows different behavior during heating and cooling representing the thermal strains.

Fig. 8: In-situ strain results (ID15A) during thermal cycling (a) of AlSi7Mg/SiC/70p in (b) matrix Al, (c) matrix Si and (d) SiC reinforcement in orthogonal orientations.

Fig. 9: Micro stresses in the matrix during thermal cycling of AlSi7Mg/SiC/70p calculated from ID15A measurements. Matrix micro stresses in the first 2 cycles (RT – 400 °C) compared to matrix micro stresses after 5 further cycles. The stress relieve in Si at the beginning of cooling is marked by A. The zero stress level approaching RT is marked by B.

Fig. 10: In-situ neutron diffraction show the micro stresses during thermal cycling (a) in AlSiC: (b) monomodal SiC (Ø ~ 100 µm) with pure Al matrix, (c) with AlSi7 matrix compared with (d) bimodal SiC (Ø ~ 5 + 100 µm) with AlSi7 matrix. The zero stress cooling stage is marked B.

Fig. 11: The voids in AlSi7Mg/SiC/70p located between big SiC particles in trimodal size distribution in an ID15A tomography (1.4 µm)³/voxel with transparent matrix (a), the same group of voids at RT (b), 400 °C (c) and after cooling again close to RT (d).

Fig. 12: Results of void segmentation of an ID15A in-situ tomography (1.4 µm)³/voxel of an AlSi7Mg/SiC/70p composite during thermal cycling (a). The voids volume fraction in (b) gauge volume of 0.3 mm³ is compared with (c) volume changes of a selected group of voids.

Fig. 13: The same group of voids (Fig.11) in the center of a bigger region (200 µm)³ after the first cycle (RT – 400 °C – RT) (a) and after 25 cycles (b), when the void volume fraction at RT increases 10 times of its initial condition, (1.4 µm)³/voxel, ID15A.

Fig. 14: Void volume fractions during heating and cooling (RT – 350 °C) in monomodal (Ø ~ 50 µm) SiC reinforced Al with and without Si content in the matrix.

Fig. 15: Al/SiC/60p monomodal at RT (a) at 350 °C (b), (0.6 µm)³/voxel, ID19.

Tables

Table 1: Investigated AlSiC samples

Composite	Matrix	SiC particle sizes	Vol. frac.	Production	Dimension
AlSi7Mg/SiC/70p	AlSi7Mg	trimodal Ø ~ 5 – 80 µm	70 vol.%	gas pressure infiltration	(1.5 x 1.5 x 10) mm³
Al/SiC/60p	Al 99.5%	monomodal Ø ~ 30 µm, 100µm	60 vol.%	squeeze casting	d ~ 0.8 mm, l ~ 10 mm for synchrotron tomography and diffraction d ~ 6 mm, l ~ 10 mm for neutron diffraction
Al/SiC/70p	Al 99.5%	bimodal Ø ~ 5 + 100	70 vol.%		
AlSi7/SiC/60p	AlSi7	monomodal Ø ~ 30 µm, 100 µm	60 vol.%		
AlSi7/SiC/70p	AlSi7	bimodal Ø ~ 5 + 100	70 vol.%		

Figure 1

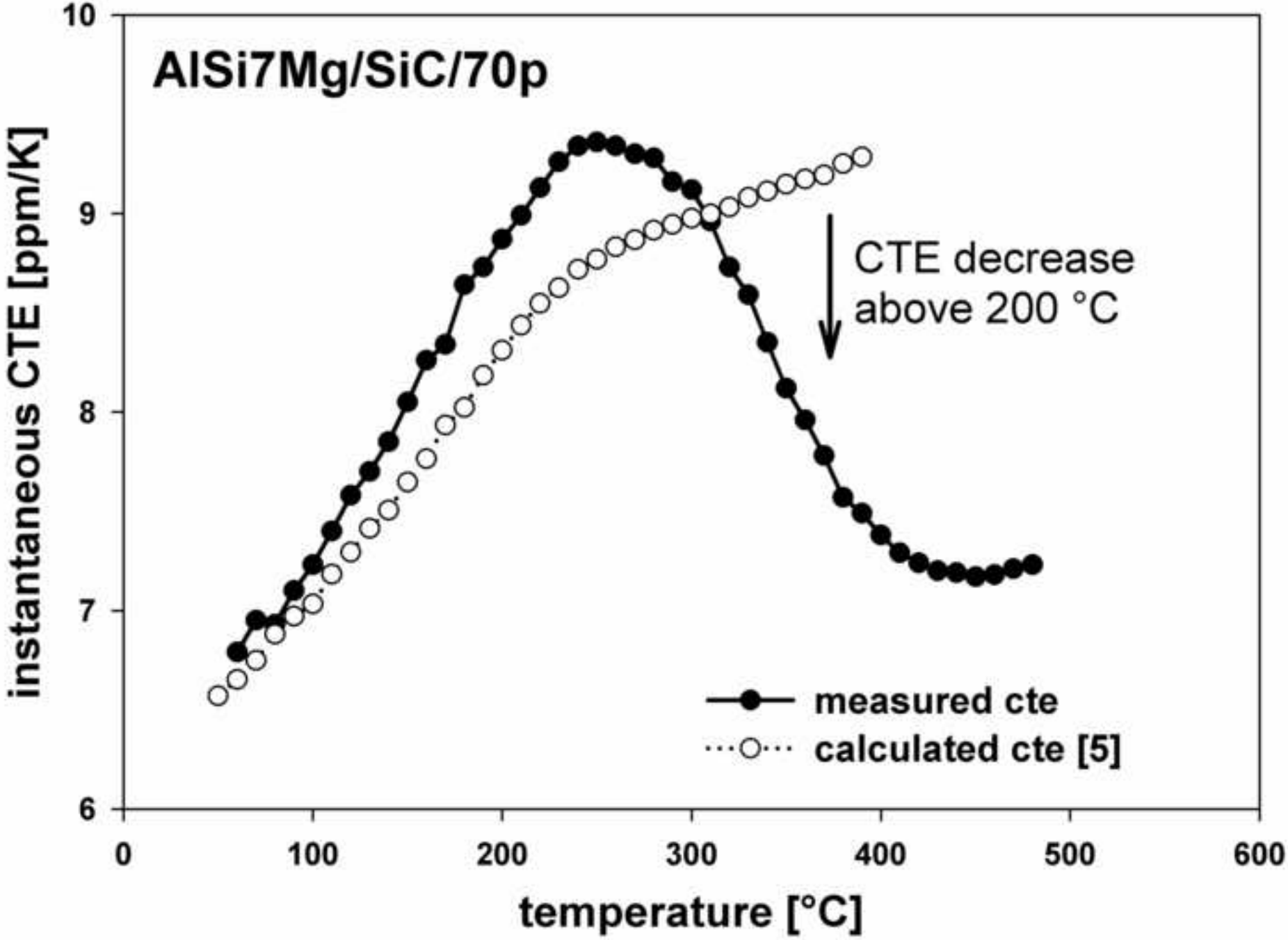

Figure 2a

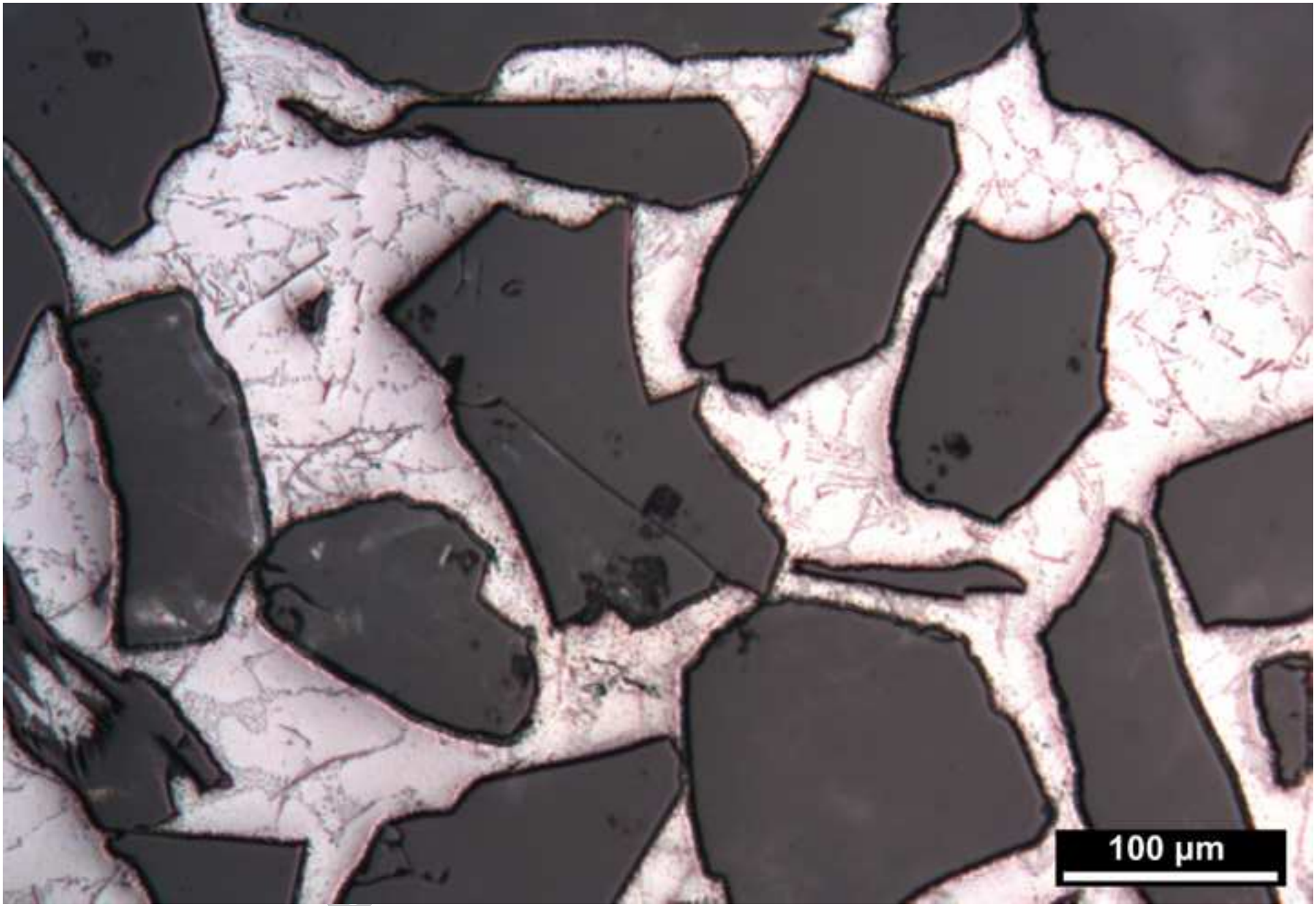

Figure 2b

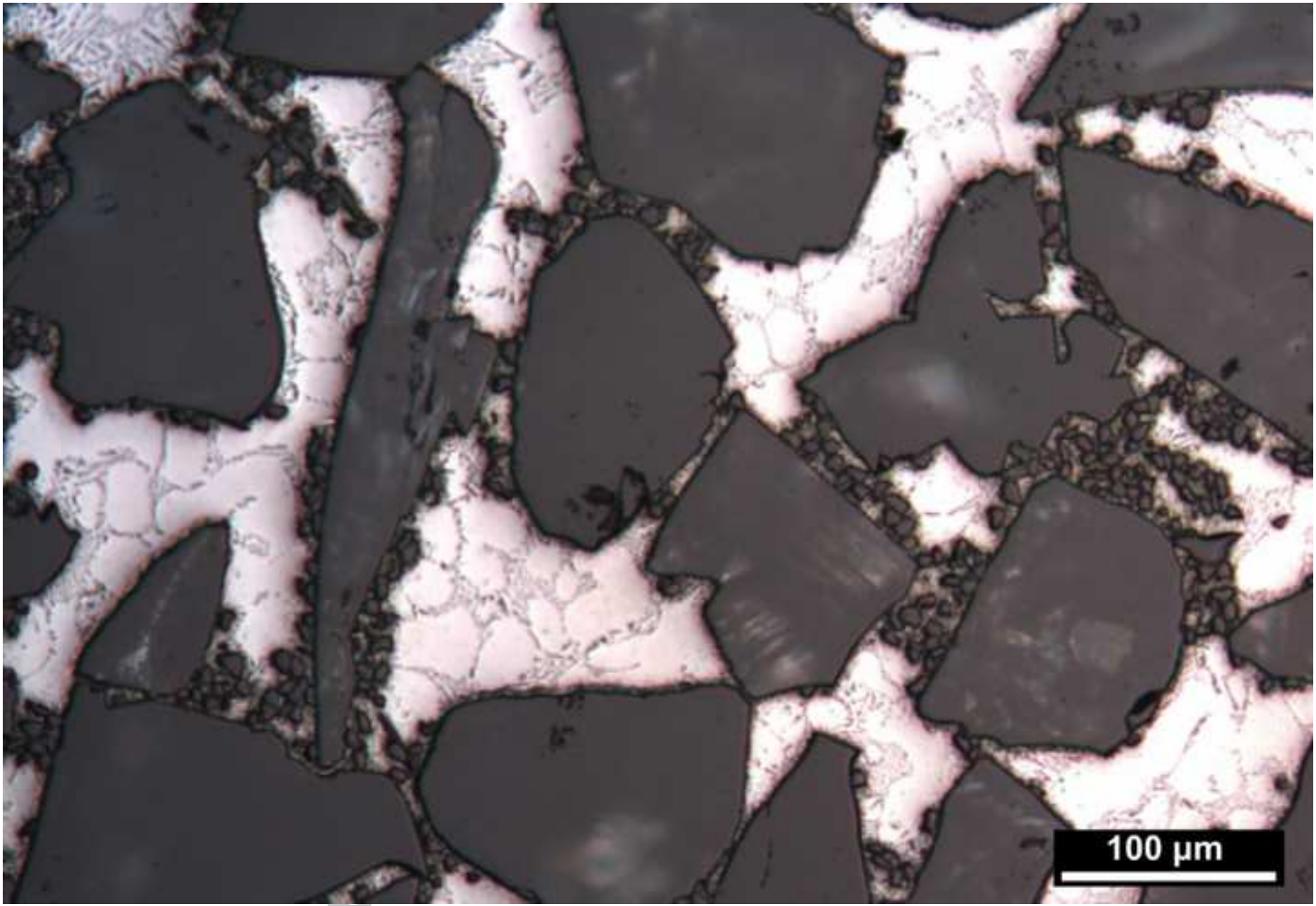

Figure 3a

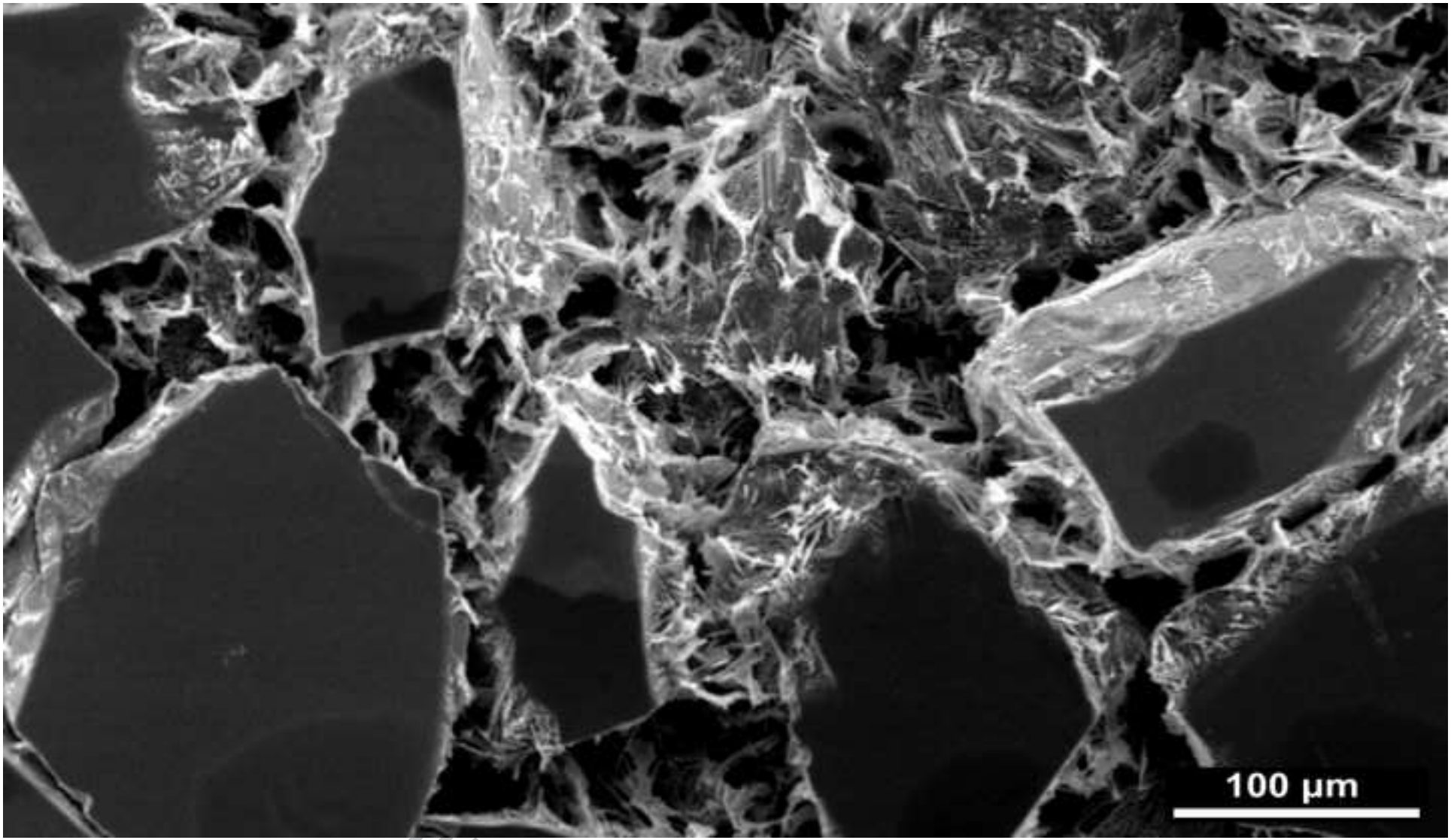

Figure 3b

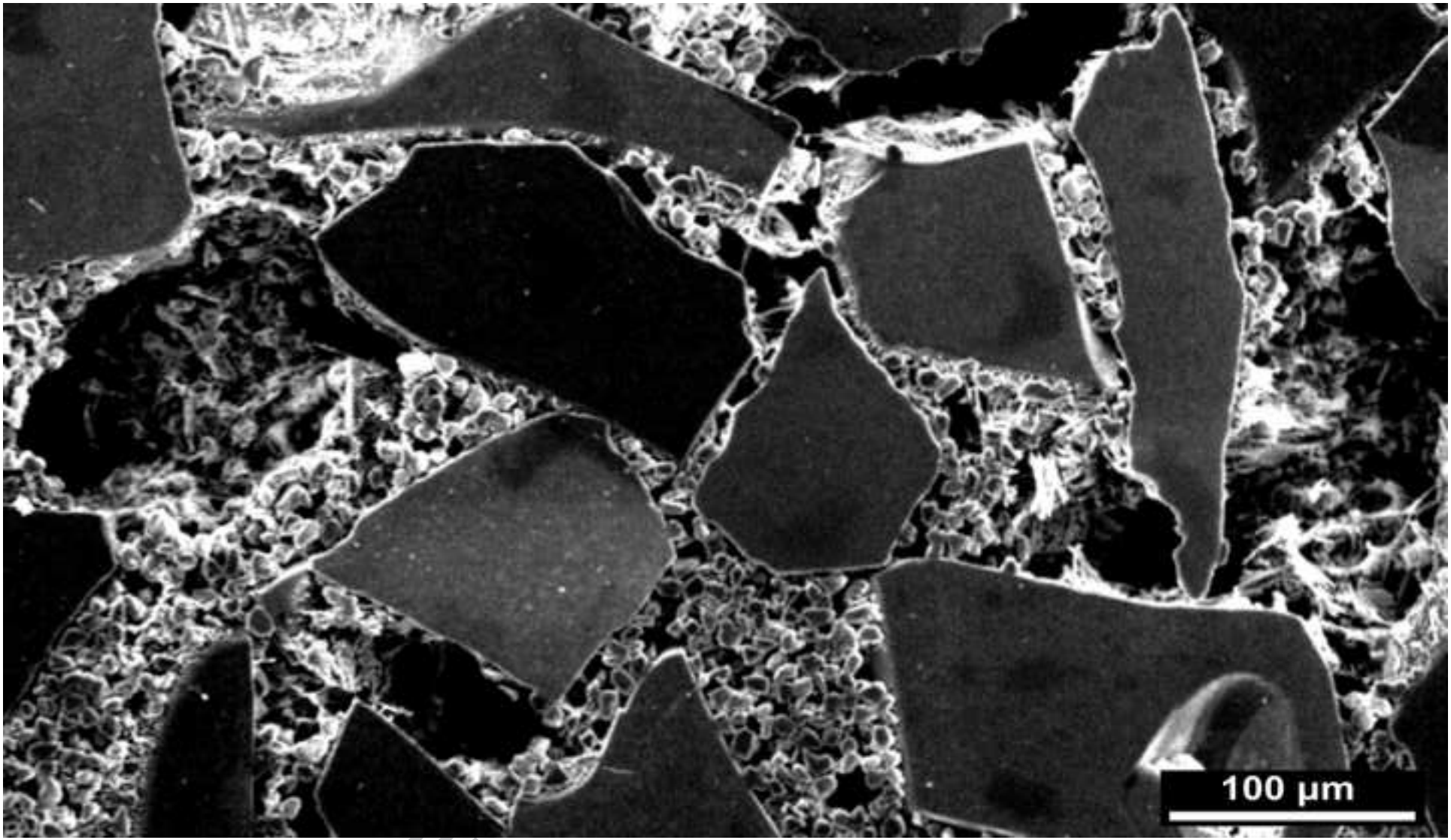

Figure 4

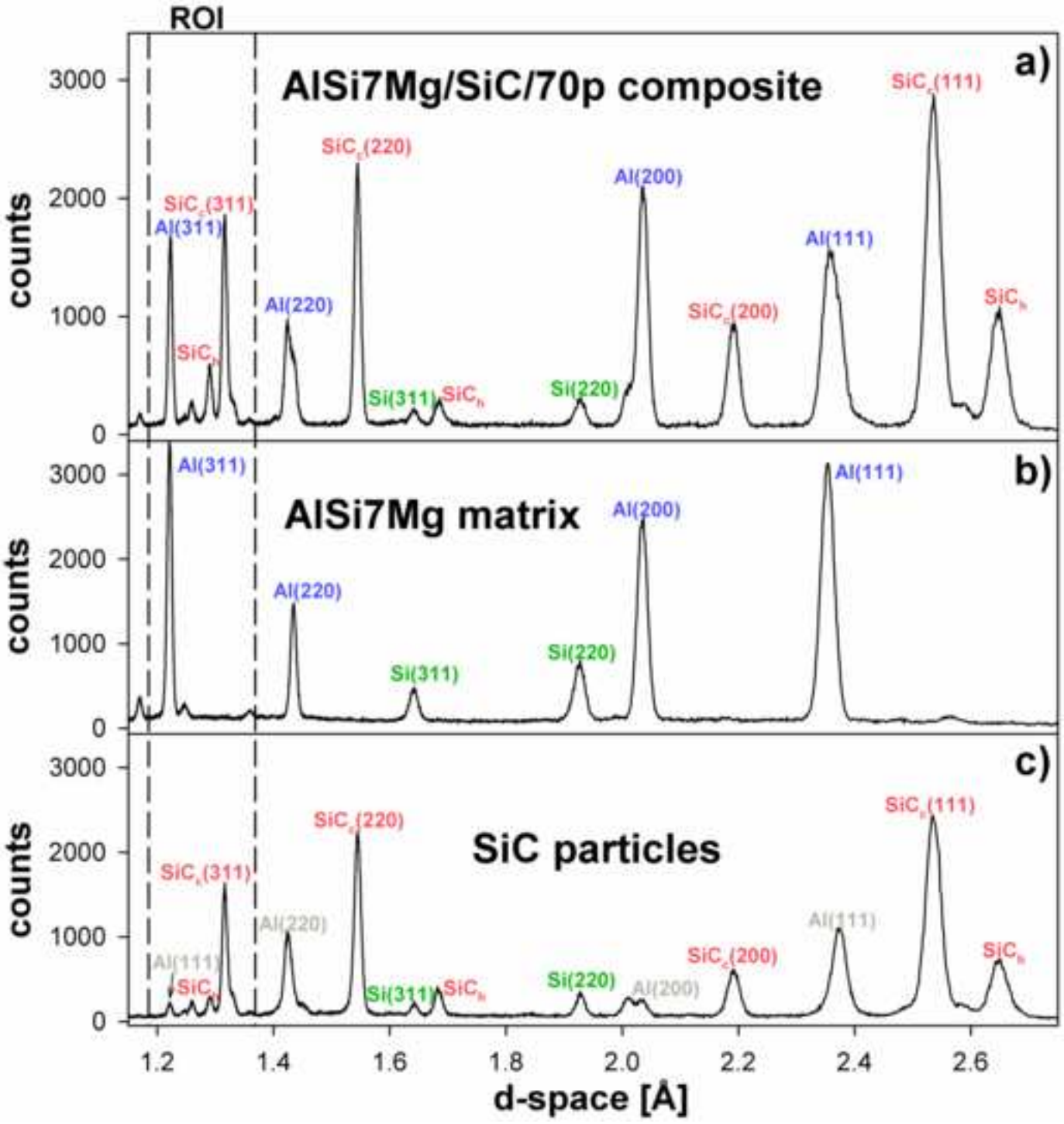

Figure 5

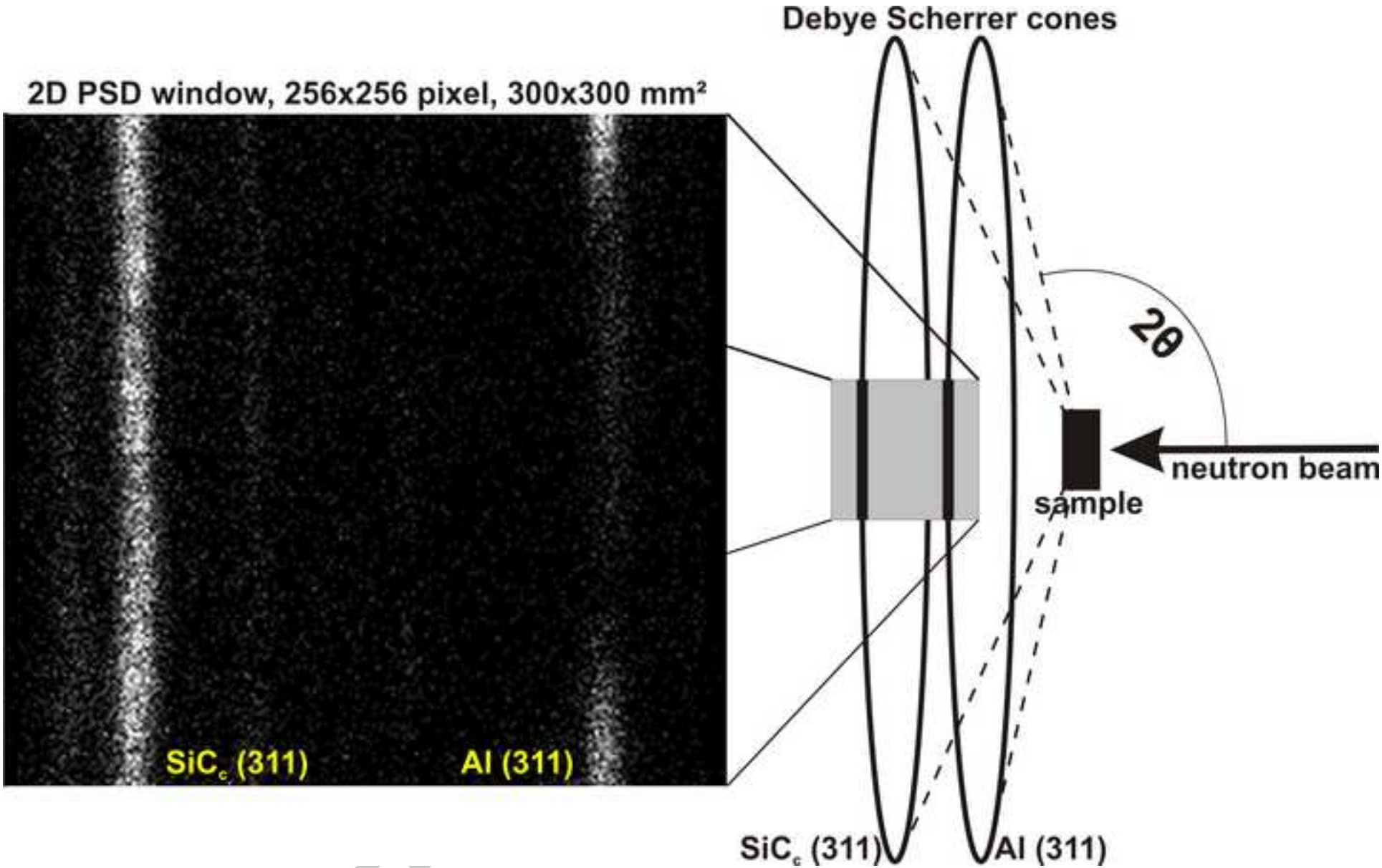

Figure 6

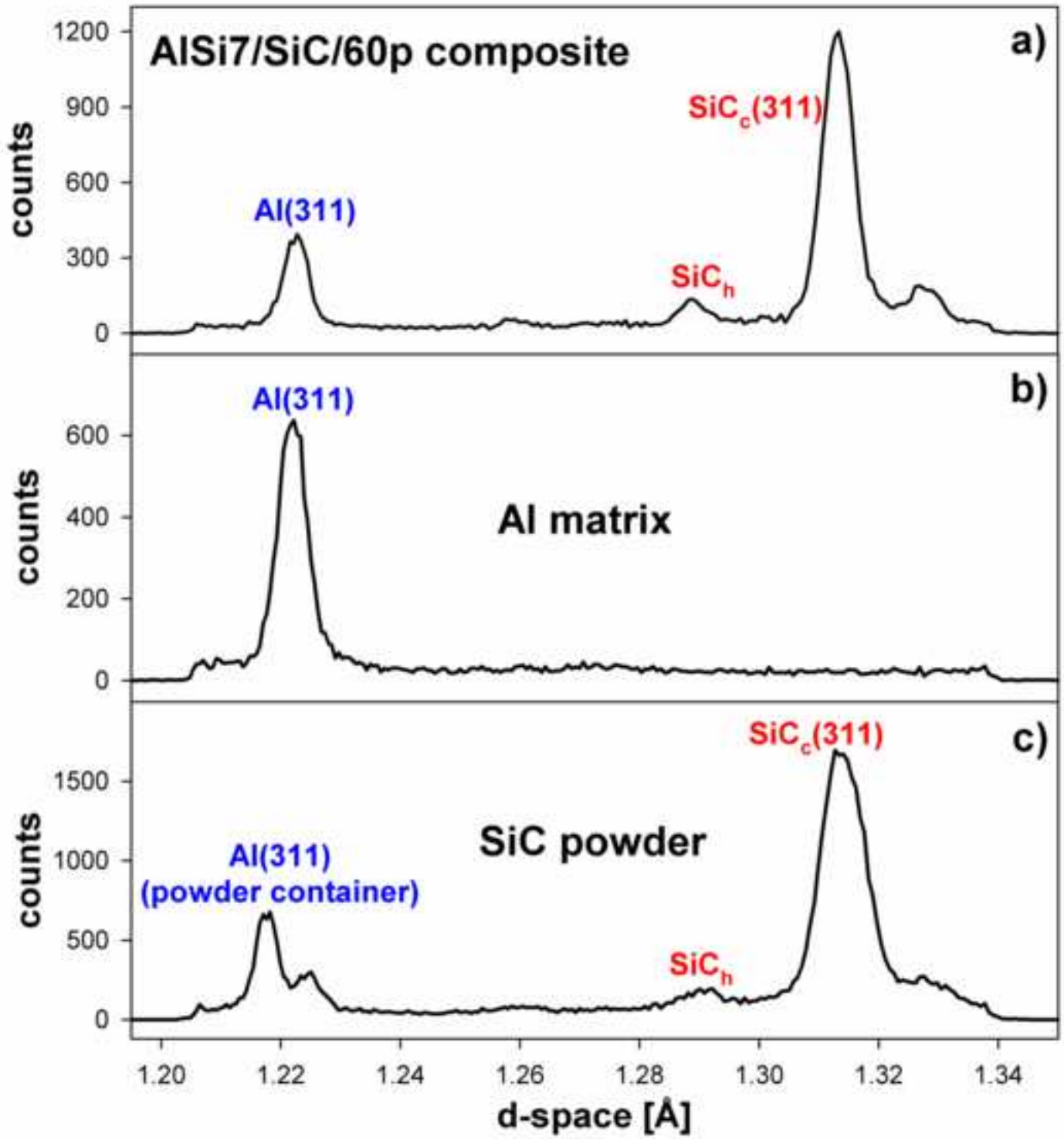

Figure 7

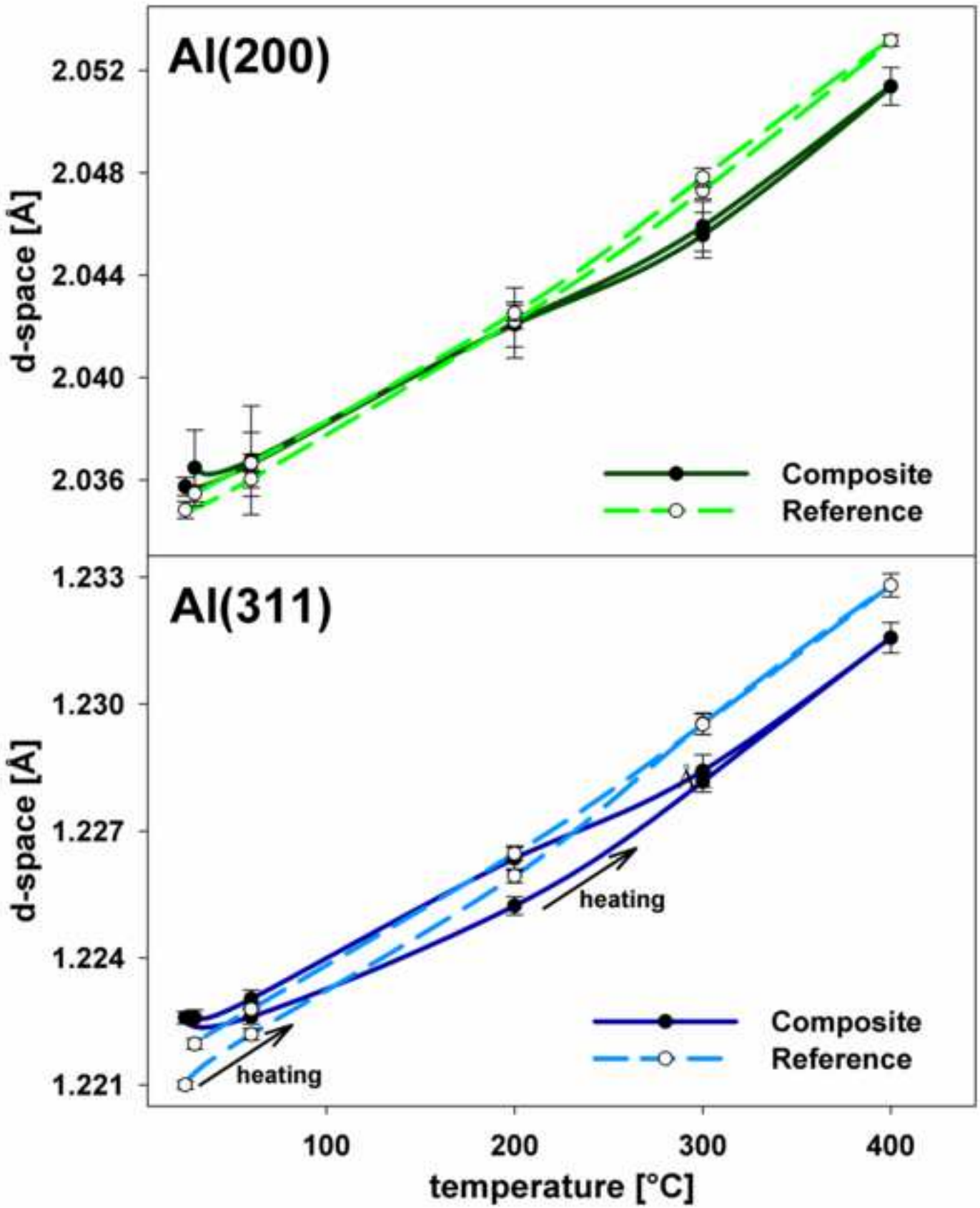

Figure 8

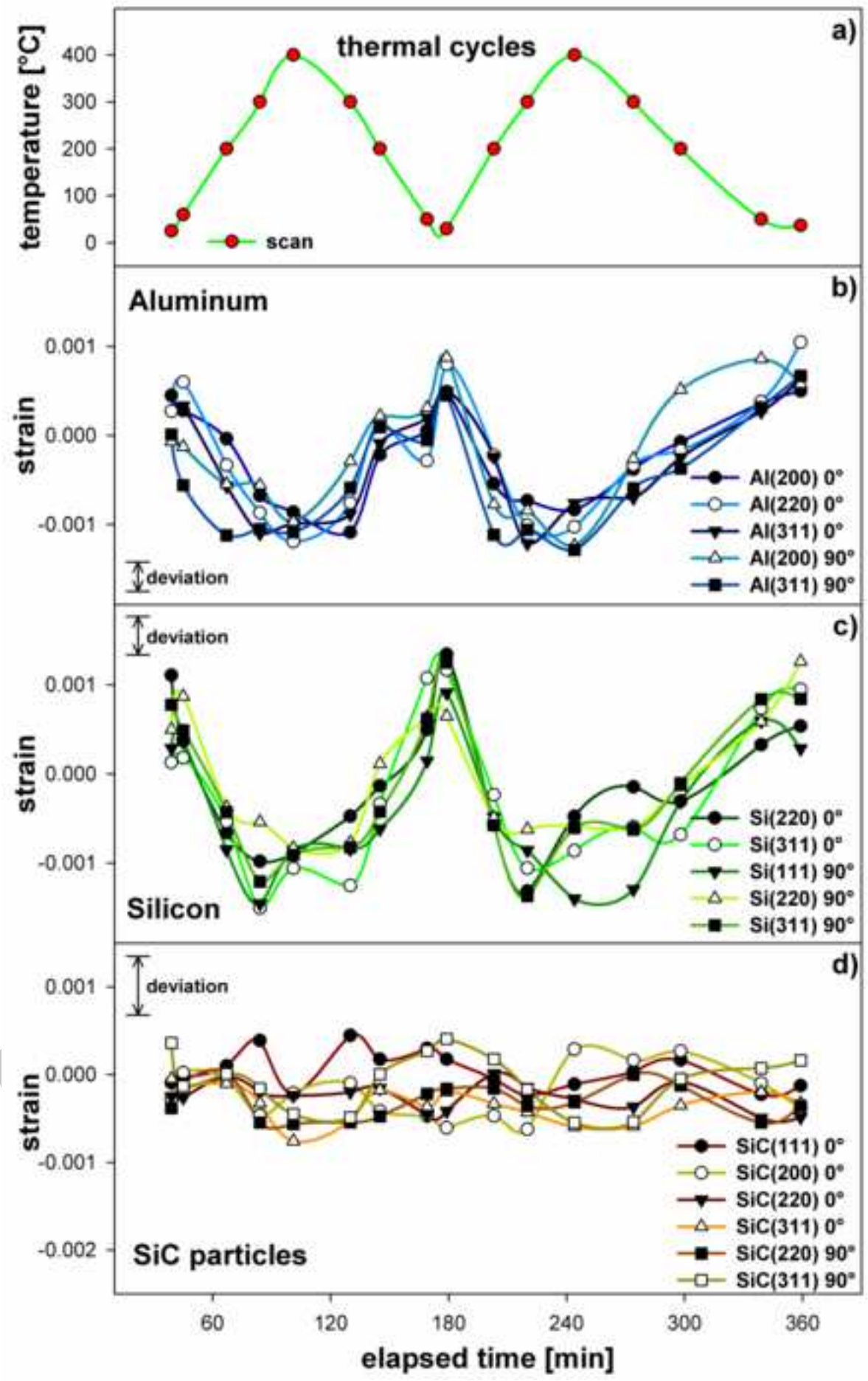

Figure 9

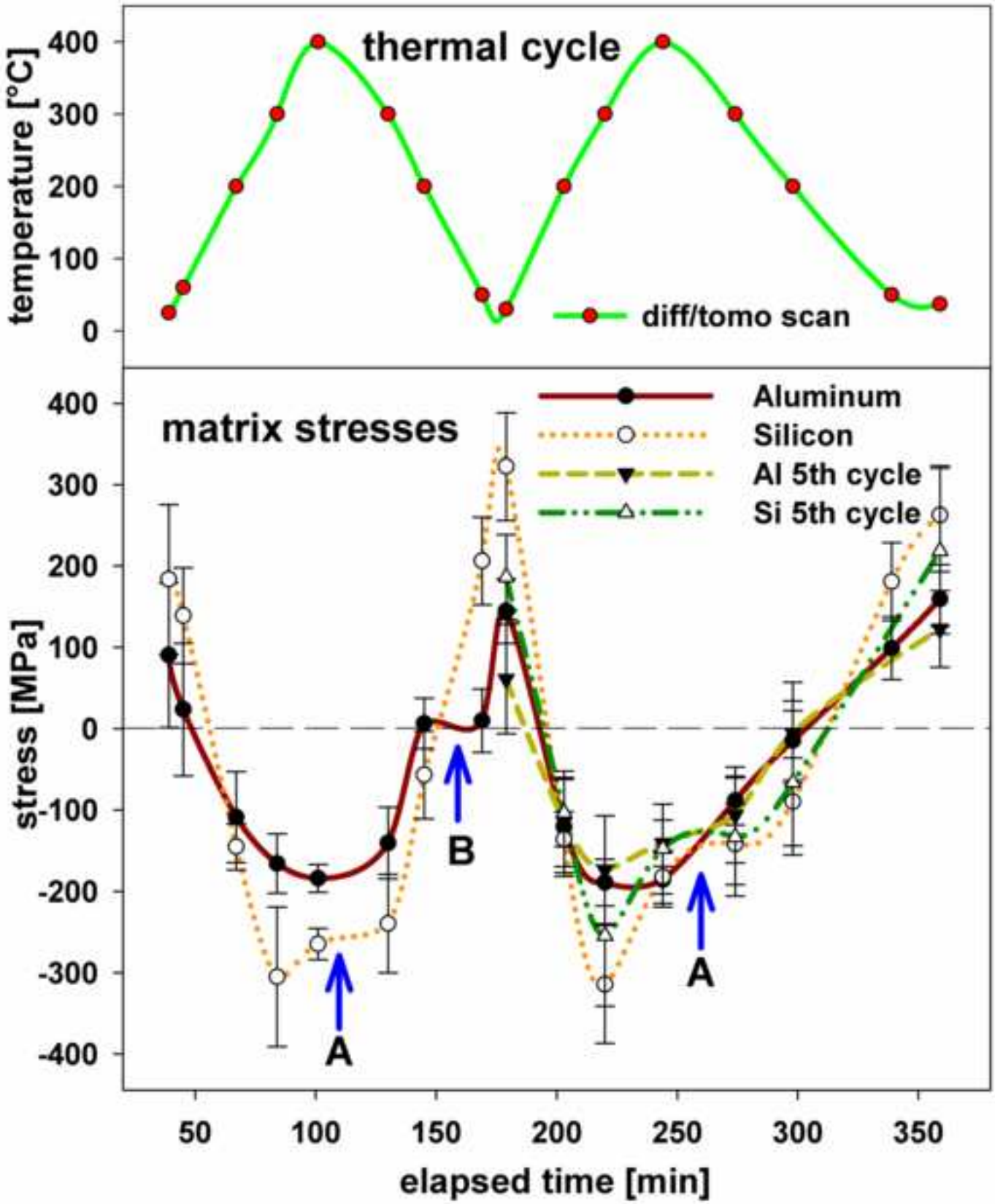

Figure 10

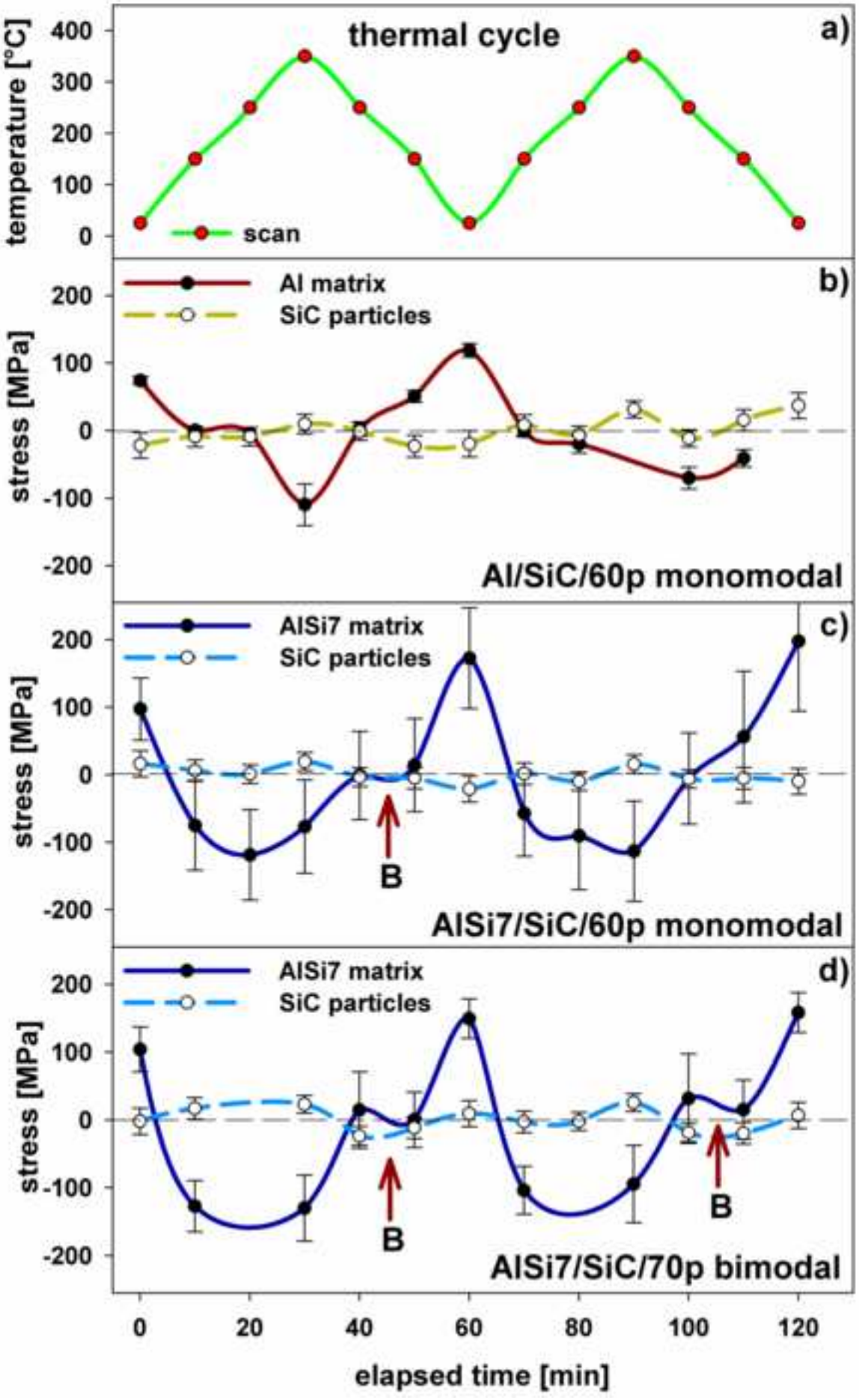

Figure 11a

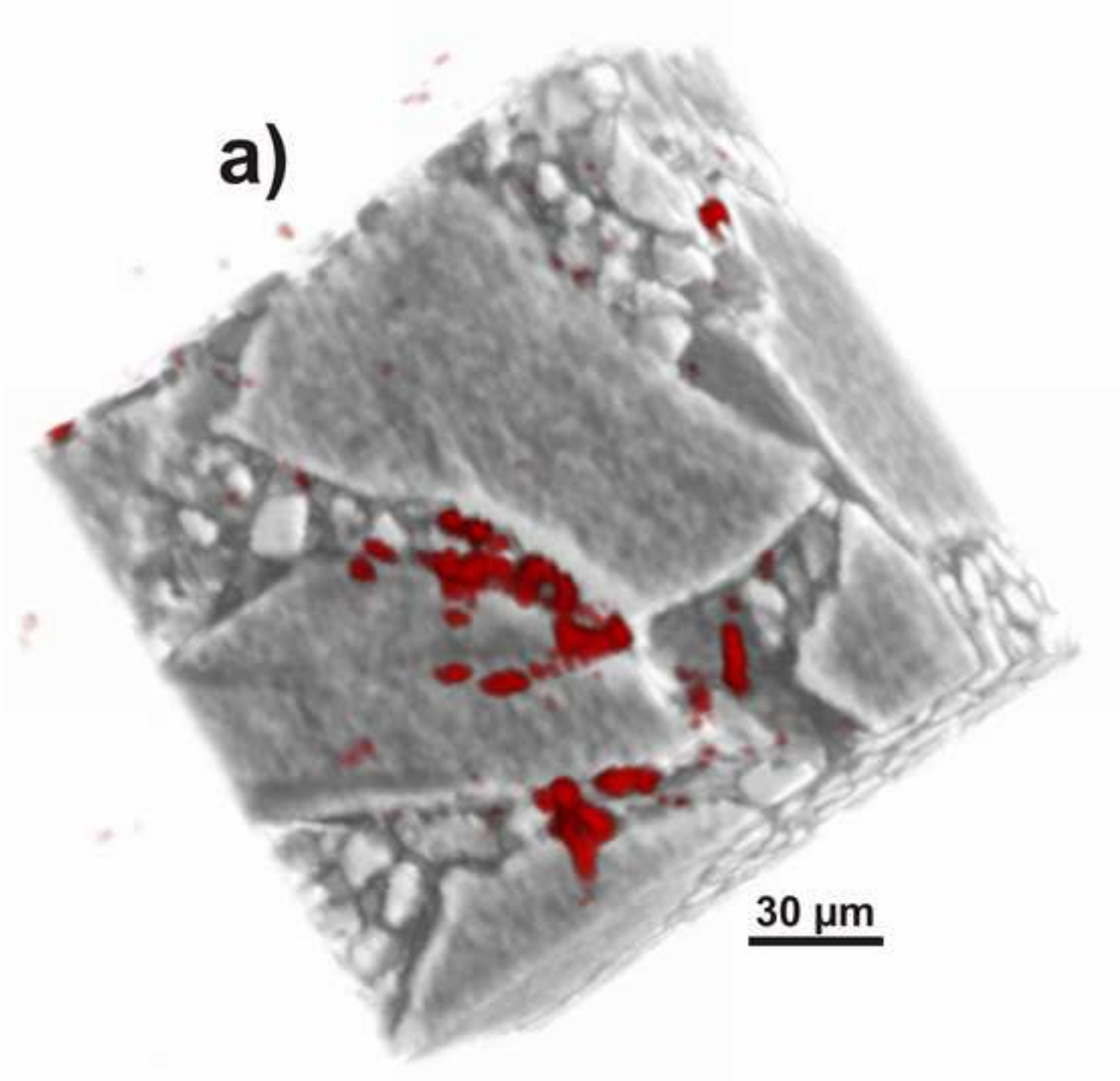

Figure 11bcd

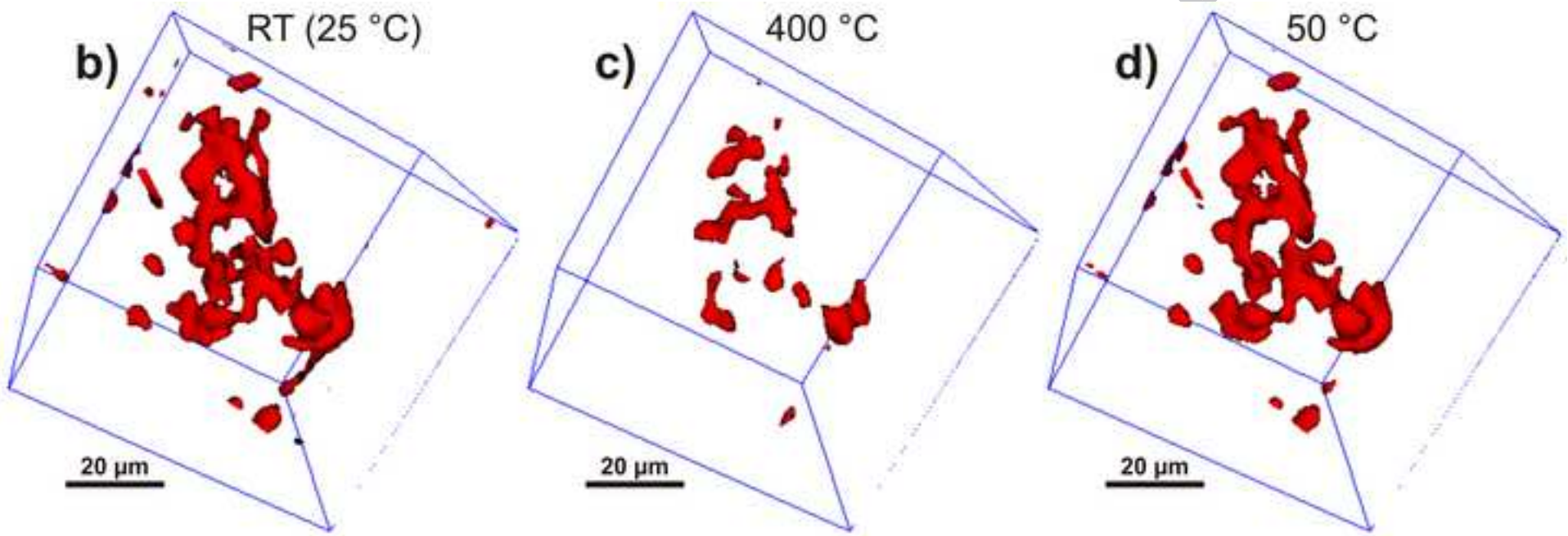

Figure 12

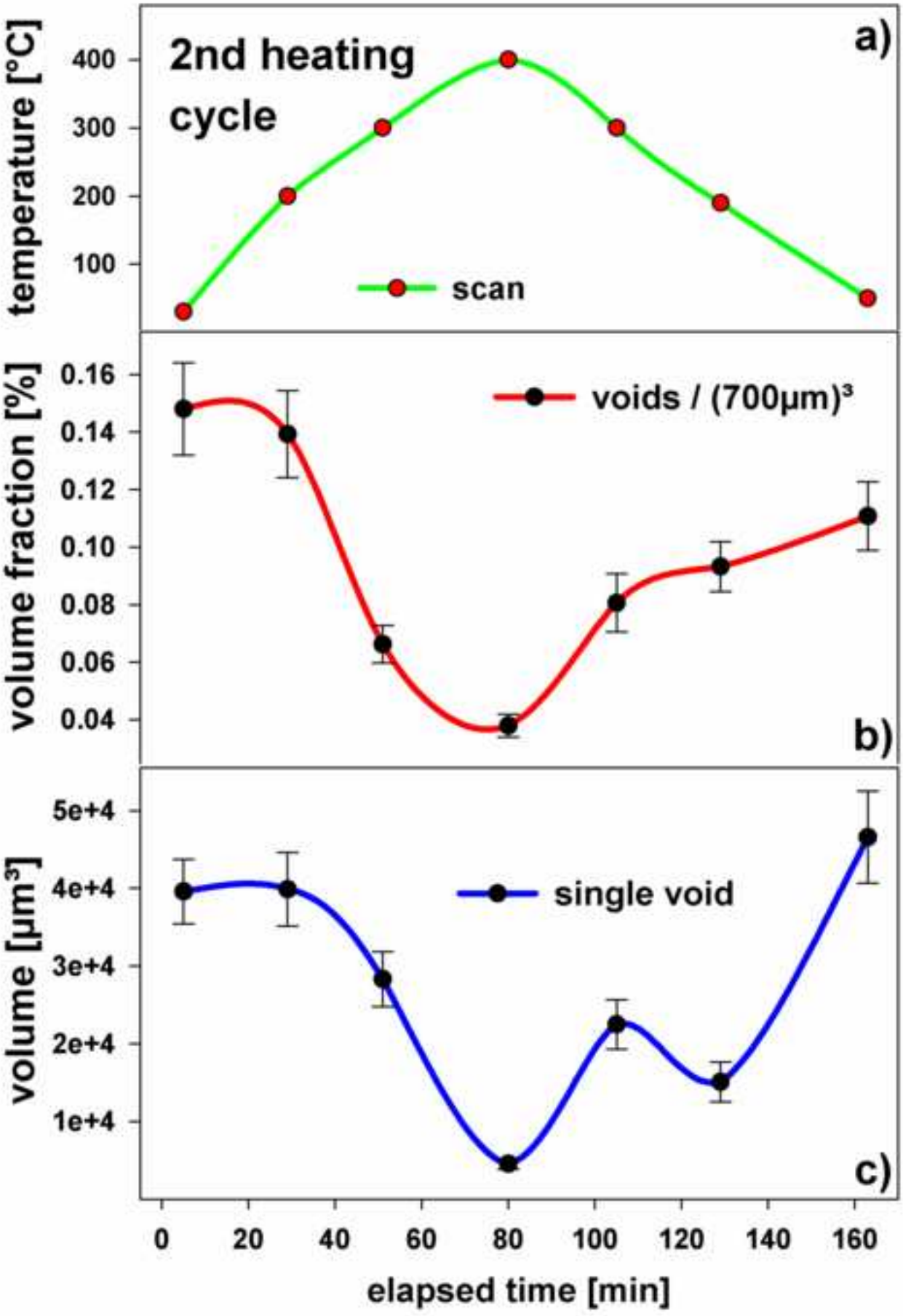

Figure 13a

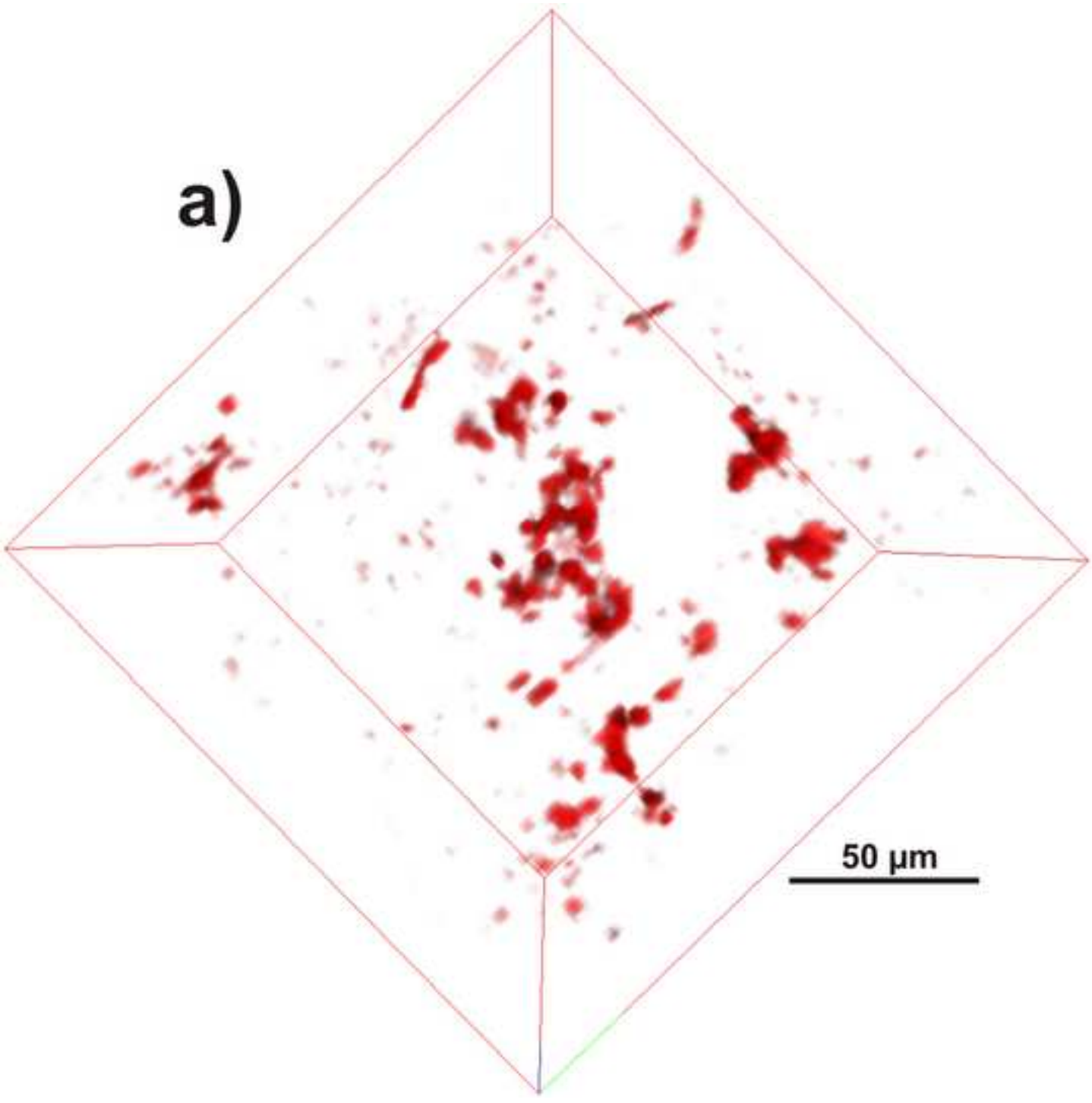

Figure 13b

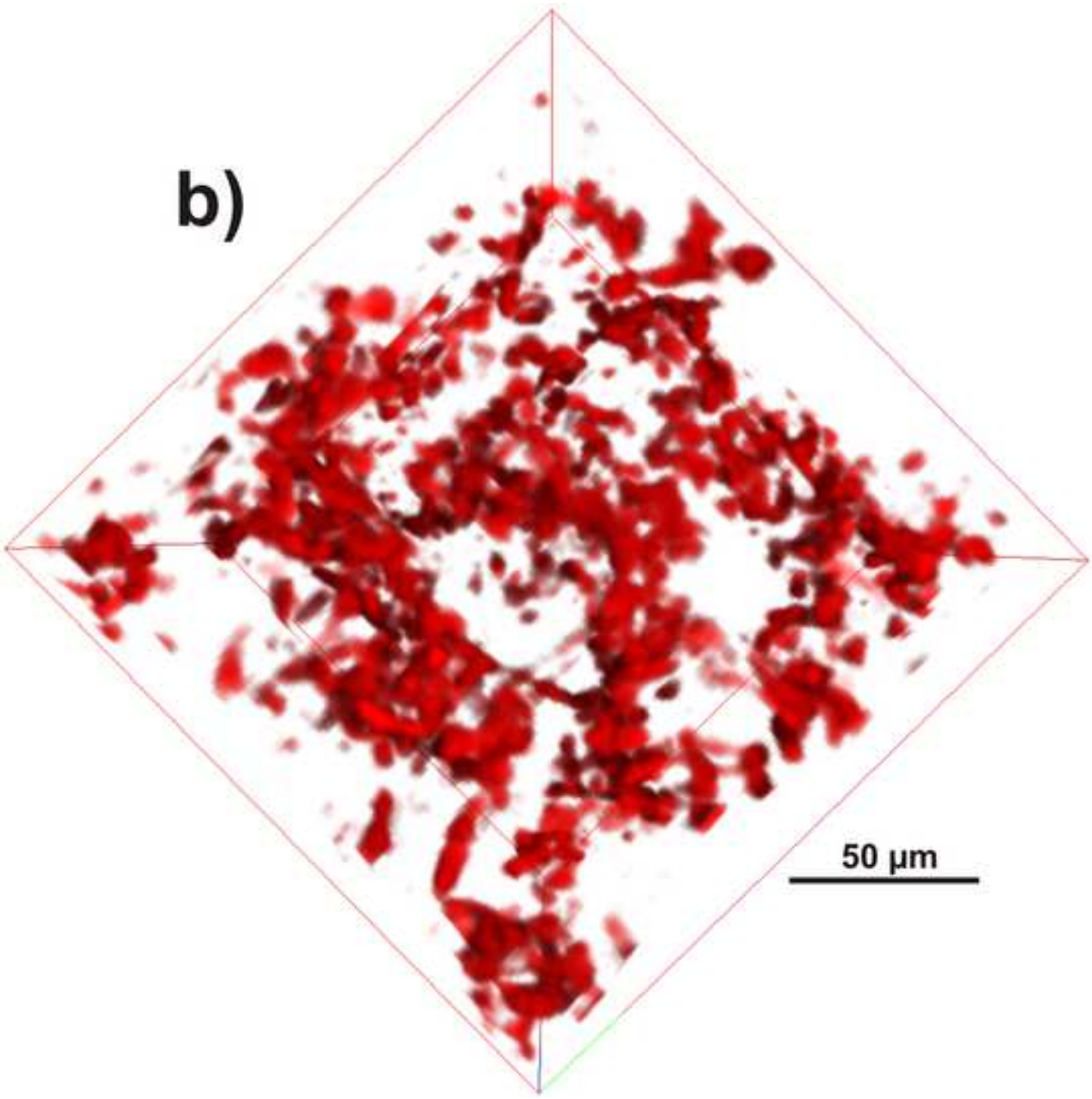

Figure 14

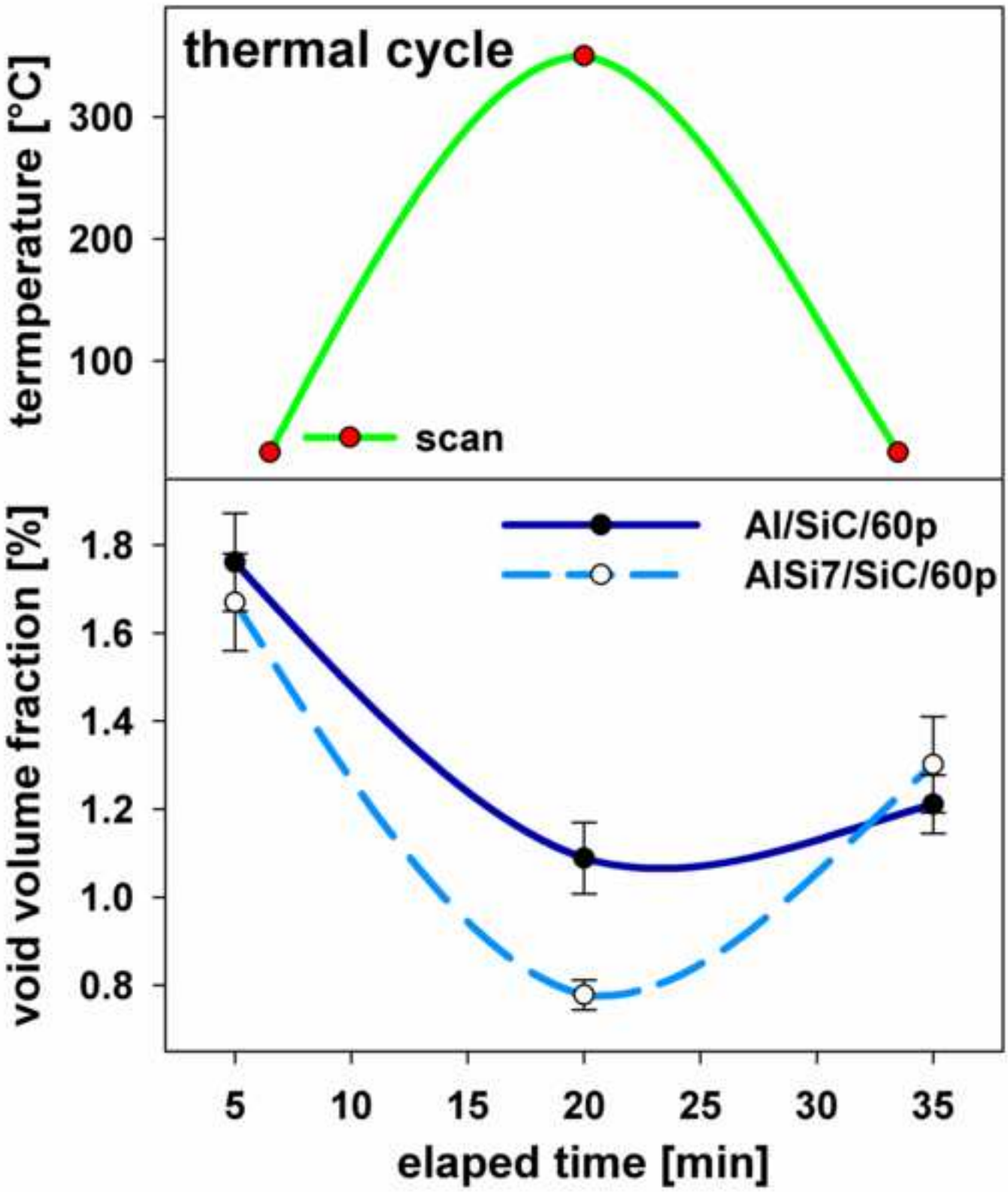

Figure 15